RIVER RESEARCH AND APPLICATIONS

River Res. Applic. (2013)

Published online in Wiley Online Library
(wileyonlinelibrary.com) DOI: 10.1002/rra.2701

AN AUTOMATED APPROACH TO EXTRACTING RIVER BANK LOCATIONS FROM AERIAL IMAGERY USING IMAGE TEXTURE

P. MCKAY* AND C. A. BLAIN

Oceanography Division, Naval Research Laboratory, Stennis Space Center, Mississippi, USA

ABSTRACT

A fundamental challenge in river analysis and modelling is the lack of readily available and reliable information on river bank geometry. Traditional survey methods are expensive and time consuming and often difficult to execute in many river systems because of hazardous terrain or lack of access. However, as high quality aerial and satellite imagery becomes available for more of the globe, it is increasingly possible to extract these bank locations directly from imagery. The most direct method of doing this involves manually designating edges based on visual criterion. This, however, is often prohibitively time consuming and labour intensive, and the quality is dependent on the individual doing the task. This paper describes a quick and fully automated method for locating water surface and river banks in high resolution aerial imagery without recourse to any multispectral information, by segmenting based on the local entropy of the image. This method is demonstrated on imagery of several rivers and its advantages and limitations are discussed. Published 2013. This article is a U.S. Government work and is in the public domain in the USA.

KEY WORDS: remote sensing; rivers; Shannon entropy; shoreline

Received 12 September 2012; Revised 8 May 2013; Accepted 23 July 2013

INTRODUCTION

Efforts to develop accurate two and three dimensional river models (see e.g. Pasternak *et al*., 2003; Novikov and Bagtzoglou, 2006; Yang *et al*., 2006) are often hampered by the lack of high quality surveyed river bank geometries. Unlike for coastlines, there is no readily accessible database of river bank locations and what information is available is often outdated and of questionable accuracy and resolution. Many rivers of interest are often located in inaccessible areas where traditional surveying techniques are of limited use or where access is otherwise denied.

In recent years, the public availability of high quality aerial and satellite imagery has greatly increased, and ever larger swaths of the globe are covered with high resolution imagery. This has opened up many avenues for using remotely sensed imagery to monitor, and develop models of, remote or unsurveyed rivers (see e.g., Winterbottom and Gilvear, 1997; Westaway *et al*., 2003; Gilvear *et al*., 2004; Legleiter *et al*., 2004; Marcus and Fonstad, 2007; Vericat *et al*., 2009). The most common method of converting these photographs into discreet river edges is to have a trained technician carefully trace the edges on the basis of visual cues. This, however, can be quite time consuming and labourious, and the quality of the final result is controlled by the skill and biases of the individuals involved.

*Correspondence to: P. McKay, Oceanography Division (Code 7322), Naval Research Laboratory, Stennis Space Center, Mississippi, USA.
E-mail: paul.mckay@nrlssc.navy.mil

The automated detection and extraction of features in remotely sensed imagery, including water and shorelines, is a major topic of ongoing research and development. Many methods have been proposed through the years, all of which perform well in certain circumstances and have certain limitations. One of the most common approaches is to use information encoded in multispectral imagery to, for instance, separate the differences in infrared reflectivity between different surfaces, such as water and land (Kelley *et al*., 1998).

Many of these techniques, unfortunately, are tied to certain spectra and thus to certain sensors and observation platforms. When such data are not available, as in cases where only visual spectrum imagery is available, other methods have been developed. The most common of these rely on segmenting the image based on differences in colour, hue, saturation or intensity between the features of interest (Gilvear *et al*., 2004; Legleiter *et al*., 2004; Tanaka, 2006). These methods are generally considered to be supervised classification techniques in that they require the active input of a trained analyst to define the characteristics of the regions of interest.

Often, however, only one image band is available, as in the case of greyscale imagery, or the features of interest are such that even a trained analyst has difficulty in defining the criteria for segmenting the image. For these cases, certain automated, unsupervised (or minimally supervised), image classification schemes have been developed using the high resolution information encoded in a single channel image to segment it into finer blocks than a human can segment it.

Segmentation by image clustering, the location and definition of regions of similar characteristics, is quite common, especially using the K-Mean or Iterative Self-Organizing Data Analysis techniques. But these techniques suffer limitations in requiring significant operator input in the setup phase, requiring significant computation time and in having difficulty in identifying geometrically straight features (Jensen, 1996). Although these techniques have been used successfully to segment water and land and determine the shoreline (Alphan, 2005), their use has been limited by speed and by the need for a trained operator. Certain more automated techniques, for example the Syneract method (Huang, 2002), have been developed to reduce the need for operator input, but they are still slow and have generally been used in segmenting land use and vegetation rather than in developing a shoreline.

The machine vision community has developed a number of powerful techniques based on the field of texture analysis (Tuceryan and Jain, 1998) that have seen some adoption by the remote sensing community. Images may be segmented by breaking them down into fundamental units, or tokens, (Tuceryan and Jain, 1990) or by comparing statistics of image ÒroughnessÓ based on frequency domain transformation (Viyas and Rege, 2006), moment-based segmentation (Tuceryan, 1994), image entropy (Singh and Singh, 2008; Pharwaha and Singh, 2009) or a combination of techniques (Awate *et al*., 2006).

This paper describes a new technique, developed at the Naval Research Lab, which automatically extracts river and river bank locations from arbitrarily sourced high resolution (~1 m ground sample distance) single channel imagery without recourse to multi-spectral or even colour information. This method relies on quantifying the difference in image texture between the relatively smooth surface of the river water and the rougher surface of the vegetated land or built environment bordering it and then segmenting the image into high and low roughness regions. The interface between the low and high roughness areas defines the river banks.

In the paper to follow, the Method Section will discuss the method and its implementation. The Validation Section will validate the technique on images of several rivers. Finally, the Discussion Section will discuss its uses and limitations.

METHOD

The new image segmentation technique to be described exploits the fact that in imagery of many rivers there is a clear difference in the roughness of the surface of the water and the roughness of the vegetated or built environment surrounding it. This difference is intuitively obvious to a human observer, allowing a human to perceive the river regardless of whether the imagery is in true colour, false colour, infrared, greyscale or any other colour space. This technique requires no information other than that contained in a single channel (i.e. greyscale) image. It is designed to work with high resolution imagery from any source, including such publicly available sources as Google Earth, Worldwind or Terraserver with no a priori requirements as to image format, size, colour space or sensor used. It is further designed to run automatically, with no operator supervision, and quickly.

Image entropy

Roughness in an image is represented by the local variance in the image colour or grey level and can be expressed in several forms. Shannon entropy (Shannon, 1948) is a metric commonly used in information theory and texture analysis that lends itself well to classifying this sort of image. The concept of Shannon entropy was developed for use in data compression techniques and is a measure of the unpredictability in a variable across a discreet set of values. It is defined, mathematically, as

$$H = -\sum_{i=1}^{N} p(X_i) log_2 p(X) \tag{1}$$

where H is the entropy of the variable with discreet values $X_1 - X_N$, N is the number of discreet values, and p is the probability mass function of X. The probability mass function is the probability that a random variable will exactly equal a discreet value, that is, the fraction of the total number of variables with any given value. In information theory, this number, H, represents the number of bits needed to encode a string, whereas in image analysis, it is a measure of the randomness inherent in an image region.

In our case, we have chosen to work with greyscale imagery with 128 discreet grey levels running from 0 to 127. The 'roughness' then associated with any pixel in the image is related to the Shannon entropy of that pixel and the pixels that surround it. Consider the case of a pixel with a grey value of 2 surrounded by 8 pixels with grey values of 1, 1, 1, 2, 3, 4, 5, 5. The calculated Shannon entropy for that 9 pixel region is then

$$\begin{aligned} H = -\big[&(0.333 log_2(0.333)) + (0.111 log_2(0.111)) \\ &+ (0.222 log_2(0.222)) \ldots + (0.111 log_2(0.111)) \\ &+ (0.111 log_2(0.111)) + (0.111 log_2(0.111))\big] \end{aligned} \tag{2}$$

and $H = 2.41938$. Normalizing by the number of values involved, (9) gives a normalized Shannon entropy of 0.26882. This value describes the level of variability in the set but does not address the range of variability. An image segment where the values vary over a small grey range is likely to depict a less rough area than one where the values

DOI: 10.1002/rra

vary over the entire grey range. Thus, we normalize this value by multiplying by the range of values in the sample, here 5, and dividing by the maximum possible value range, 128, to define a normalized Shannon entropy or H_n. This gives us a value of $H_n = 2.41938 \times (1/9) \times (5/128) = 0.0105$ as the field and range normalized Shannon entropy. This value serves as a good indication of local variability and thus roughness.

Our final formulation then is for a field and range normalized Shannon entropy defined as

$$H_n = -\sum_{i=1}^{N} p(X_i) log_2 p(X) \left(\frac{1}{s}\right) \left(\frac{r_l}{r_m}\right) \quad (3)$$

where s is the number of pixels being analyzed, r_l is the local range of values across the pixels and r_m is the maximum possible range of values.

Algorithm

Imagery must first be obtained from some source. This imagery must be of high enough resolution that the rough surface of the land can be readily observed. This required resolution will vary depending on the location of the area of interest, but it will generally be in the range of 1–3 m per pixel. If the imagery is not already georeferenced, there must be sufficiently defined features in the image such that the locations of two points (three if the image has not been orthorectified) are known precisely both in image coordinates and in geographic coordinates (i.e. Universal Transverse Mercator or lat/lon). This is necessary to map the extracted data back to Earth coordinates. Figure 1 shows an example of imagery, which meets these criteria. This image is 1 m resolution visual spectrum imagery of the Pearl River near Stennis Space Center from the Louisiana State University Computer Aided Design & Geographic Information Systems Lab, Baton Rouge, LA (http://atlas.lsu.edu) .

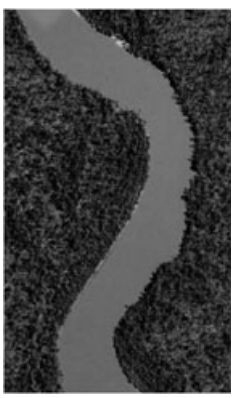

Figure 1. Example imagery of the Pearl River, LA. Image data distributed by 'Atlas: The Louisiana Statewide GIS'. Louisiana State University Computer Aided Design & Geographic Information Systems Research Laboratory, Baton Rouge, LA, 2011 http://atlas.lsu.edu

The image must be converted to greyscale, if needed, by converting gamma values to intensity (Pratt, 1991). If the image covers a large reach of river then it is likely to be a mosaic of multiple images shot at different times and under different conditions. This can result in discontinuities in grey level at the seams between images, which can complicate analysis. If this is the case then the image must first be equalized using a random path, roving, patch equalization filter. Once patch equalized the entire image must then be equalized to occupy the entire grey range from 0 to 127.

We have chosen to analyze the images on the basis of 9 pixel kernels, that is, each pixel will be characterized by its own value and those of the 8 pixels immediately adjacent to it. This is the smallest kernel size available for centered statistics and will yield the most accurate bank locations. Increasing the kernel size would allow the technique to be applied to areas with lesser roughness on the banks at the sacrifice of location accuracy. For our 9 pixel kernels, the image must be padded by adding an extra set of mirrored pixels around the edge (Figure 2). This allows the centered statistics of Equation 3 to be calculated along the edges of the original image with no data loss.

Next, for every pixel in the original image, the local normalized Shannon entropy (Equation 3) is calculated for the nine pixel box surrounding, and including, the pixel of interest. The padded pixels are then discarded. The normalized Shannon entropy is plotted for the original image in Figure 3. Here, the range of values (0 .. 1) has been expanded across the entire greyscale range (0 .. 127) for visualization purposes.

The image is then binarized by thresholding such that all pixels with normalized Shannon entropy levels greater than a cut-off value are set to 1 and all others are set to zero. This is shown in Figure 4. For initial purposes, this cut-off value should be set to the median value among all pixels in the image. It can be manually adjusted as needed on the basis of the image and the experience of the analyst; however, we have found this value to work in all of our cases.

At this point, the image will not be completely clean. There can be holes in the water caused by small boats or

6	5	6	7	8	7
2	1	2	3	4	3
6	5	6	7	8	7
10	9	10	11	12	11
14	13	14	15	16	15
10	9	10	11	12	11

Figure 2. An example of image padding. The original image is shown by the intensity levels depicted in the grey cells. The clear cells represent mirrored image padding added around the edges of the original image

DOI: 10.1002/rra

Figure 3. The distribution of Shannon entropy calculated from Figure 1 using Equation 1. Dark colours represent low entropy values (smooth regions), whereas light colours represent high entropy values (rough regions)

islands or rough patches tied to sun glint or ship wakes. Similarly, there can be small areas of speckle in the land due to small regions of visually smooth land, pavement, vehicles and the like. These must be eliminated. An automated technique for removing these artefacts is based on two of the basic operations of mathematical morphology: dilation and erosion (Sera, 1983). These are operations whereby a binary image is acted upon by a structuring element of some regular size and shape. In erosion, pixels are removed from a binary structure equivalent to those masked by the structuring element with the element centre moving along the edges of the original structure. Dilation is the opposite operation. These form the basis of the operator pairs of closing and opening. Closing involves dilating and then eroding an image, whereas opening involves eroding and then dilating an image. Closing serves to remove, or close, any small holes in the image, whereas opening serves to despeckle or remove noise from the image.

For this technique, we choose a circular element with a diameter of 3 pixels. This size is selected to match the width of the 9 pixel kernel used in the entropy calculation. We have found that a single pass through, closing and opening, serves to remove all significant artefacts in our imagery. Multiple passes may be made with the understanding that each pass also serves to smooth out and average the river bank locations, removing small detail. This may or may not be a concern depending on the desired use of the edge locations later.

Figure 5 then shows the results of applying these two morphological operations to the image in Figure 4. The locations of the black (low entropy) pixels then can be returned as the location of the water. The river edges are then located by finding the interface between the low entropy (water) and high entropy (land) pixels by examining the local gradient to find the transition. These edges are plotted in white on Figure 6. As can be seen, the plotted edges show very good agreement with the edges as determined from visual inspection.

Figure 4. Thresholded and binarized version of Figure 3

VALIDATION

In order to be of use in processing river images, the technique must either be as accurate as other methods but faster and/or more robust or else the same speed as other techniques but able to handle a wider range of conditions.

Pearl River, LA

The case presented in Figures 1 and 6 represents an ideal case for demonstrating the algorithm in that the surface of the water appears uniform and nearly perfectly smooth, whereas the land is uniformly vegetated and rough; however, it is also one where a human operator would have no trouble similarly segmenting the land and the water. In order to validate this technique, these results were compared

Figure 5. Figure 4 after cleaning by using the mathematical morphology operations of opening and closing

DOI: 10.1002/rra

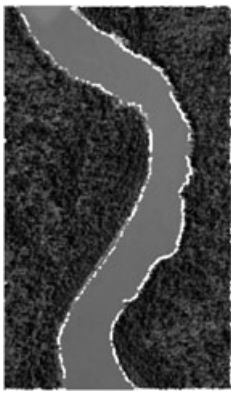

Figure 6. Edge pixels, shown in white, superimposed on the original image from Figure 1

with the edge as selected by a human operator tracing pixels. The automated technique was coded as a MATLAB script and run on a MacBook Pro with a 2.4 GHz Intel Core 2 Duo processor and 4 GB of random-access memory. The script ran in 1 min 27 s to process the 600 x 1400 pixel image. A human operator loaded the image in the open source Quantum GIS programme and traced the edges to create a ESRI shape file, which was exported for edge extraction. The process of tracing the edges took 28 min with another 8 min required to write the shape file and then extract the edges from the shape file into MATLAB (MathWorks, Nantick, MA, USA).

The two techniques produced substantially the same contour. In order to examine the difference between them, a spline was fit to each one, and for each point in the computed edge, the nearest point in the traced edge was located and the error was taken as the separation between the two in x and y. Considering the entire image, the root mean square (RMS) error between the two techniques was 0.56 pixels. The maximum error was 3 pixels where trees overhung the river bank. The automated approach traced the inside of the curve, that is, it picked up the tree tops and connected them, whereas the human operator was able to recognize this and estimate the proper bank location despite the overhang. Recognizing that 1 m resolution is not needed for most monitoring or modelling efforts, we down sampled the bank locations from the both processes to 5 m resolution and compared them. In this case, the RMS error between them dropped to 0.43 pixels.

Atchafalaya River, LA

Figure 7 shows an image of a section of the Atchafalaya River, LA, extracted from Google Earth and converted to greyscale. Visible edges are clearly seen between the image tiles, which make up the larger image and must be dealt with by the patch equalization filter. The river largely winds

Figure 7. Image of a section of the Atchafalaya River, LA. Map Data: Google, United States Department of Agriculture Farm Service Agency, Europa Technologies

through a forest, but there are nearby roads and it comes within 10 m of an urban built environment. The span of the river is much greater than in the Pearl River case. The ground sample distance is 2 m and image size is 6000 x 8000 pixels. This represents a more challenging case to the automatic processor but one which would still be easy for an operator to define

We processed the image exactly as described previously. The automated routine took 86 min and 48 s to finish, whereas a human operator took 5 h and 13 min. Although the automated process did not scale uniformly with the operator, it was still much faster. This discrepancy in scaling is due to the fact that a human operator can choose to ignore all of the pixels outside of the area of interest while the automated routine must address them all. Judicious preprocessing of the image by flagging areas away from the river to be ignored by the analysis routine will serve to speed up the automated processing if desired. Alternately, the routine can be allowed to run overnight or when no human operator is available.

Despite the lower resolution and the tile edges in the image, the two techniques produced essentially the same contour with an RMS error of 0.73 pixels between the two. The extracted edges for a zoomed detail of the river are shown in Figure 8. The roadways and built environment were picked up as being morphologically smooth and tagged as water. The 6 m (3 pixels) structuring element used in the dilation and erosion filter removed the road automatically. The built area was too large to be removed, but it was clearly separated from the river and can easily be deleted when the results are reviewed.

DOI: 10.1002/rra

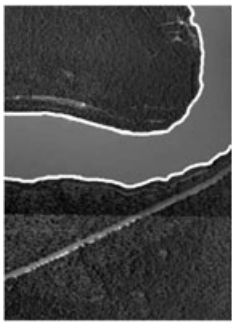

Figure 8. Edge pixels, shown in white, superimposed on a detail section of the original image from Figure 7

Snohomish River, WA

Figure 9 shows an image of a section of the Snohomish River, WA again from Google Earth and converted to greyscale. Areas outside of the immediate vicinity of the river have been set white and have been flagged with a value of −9999 indicating that the entropy processing routine should ignore them. This is carried out to increase the speed of processing when the river moves diagonally across the square image space. The ground sample distance is 1 m, and the reduced image has a total of 2.5E6 pixels. In this case, the processing is complicated by the fact that the river runs through a mixture of urban and agricultural area rather than forested area. The land near the river has several small ponds and smoothly mown fields and structures. Paved roads follow closely along the bank. There is also some amount of sun glint on the water in places as well as some small boat traffic not visible at this scale but represented in the 1 m imagery.

Processing the image as described previously, the automated routine finished in 31 min and 27 s, whereas the human operator took 2 h and 46 min. Flagging the points far from the area of interest greatly improved run time for the automated processor. Figure 10 shows the image processed for entropy, binarized, opened and closed. Black areas represent smooth regions and white ones rough (or flagged pixels). The river can be clearly seen, but there are also a considerable number of other areas highlighted representing ponds, fields and buildings. The effects of boat traffic have been removed, and the extra roughness associated with sun glint was below the threshold value and so was cut off. Extracting the edges and superimposing them on a detail from Figure 9, we see that while the automated processor does a good job of picking out the river edges it also picks out ponds and fields and bits of roadway, which are too large for the 3 pixel structuring element of the filter to remove. Increasing the element size, or adding multiple iterations of the filter, results in excessive smoothing of the river bank edges. Prior to this repeated filtering, the automated edges agree with the manually extracted edges with an RMS error of 0.45 pixels. After one more filtering operation, this error increases to 1.05 pixels. After a second filtering operation, this error increases to 2.27 pixels, and a number of the isolated smooth areas are still present and must be edited out in post processing. This suggests that if high fidelity river bank locations are required, this technique is of limited use in heavily developed or built environments without considerable manual or automated post processing to remove image artefacts (Figure 11).

Figure 9. Image of a section of the Snohomish River, WA. Map Data: Google, US Geological Survey

Figure 10. Image in Figure 9 processed for entropy, binarized, opened and closed

DOI: 10.1002/rra

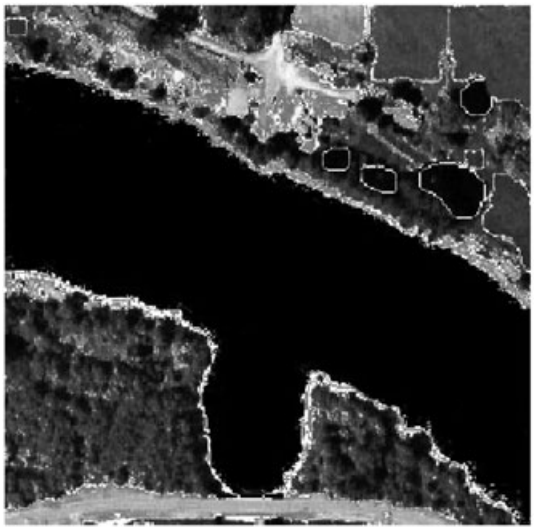

Figure 11. Edge pixels, shown in white, superimposed on a detail section of the original image from Figure 9

DISCUSSION

We have presented a new method for extracting river bank locations from high resolution aerial or satellite imagery using image texture, as measured by a normalized form of Shannon Entropy, as the metric to discriminate water from land. This technique exploits the fact that in many rivers, the surface of the flowing water appears noticeably smoother than the surrounding land, allowing us to segment them based purely on this fact. The technique represents an improvement over prior art in that it requires only a sort of least common denominator imagery, that is only greyscale visual spectrum imagery, such as is available easily, and often freely, from government and commercial providers. It is not tied to any specific platform or sensor or to the availability of any particular wavelength of spectral data. The only requirement is that it is of sufficient clarity and resolution, generally on the order of 1 m ground sample distance, that the surface texture can be clearly distinguished.

When working with high quality imagery in an area with a clear difference between water surface texture and land surface texture, the technique works quite well. On an ordinary laptop, it processes the image and extracts the edges in much less time than is required by a trained human operator, with RMS errors between the two shorelines of less than 1 pixel. Given that in many images, the exact location of a river bank can be difficult for even a human to determine down to the pixel, this places the automatically extracted banks within the error band of the human operator.

Areas of vegetation and tree canopy overhanging the river banks will cause the channel to appear narrower than it should be. This can be averaged out some by down sampling the extracted bank data and fitting a curve to the sparse points. The exact deviation of this from the true bank location can not be determined because even a human extracted bank is only an educated guess in areas where the bank is not visible. The technique is robust for cleaning small boat traffic as well as minor sun glint from the surface of the water although it may have difficulty removing large ship traffic or extensive glint from very low angle sunlight, such as is more likely to be encountered in high latitudes. The technique recognizes areas of urban or rural built environments, such as mowed fields, roadways, structures and paved lots as morphologically smooth and flags them as water. The morphological opening and closing operations will automatically remove the smaller of these features but repeated use of this filter may smooth the river banks below what is considered an acceptable resolution. This determination must be made on the basis of the desired use of the bank information and the needed end resolution. Larger of these features must be removed by in post-processing. Because of this limitation, the technique may not be suitable for use in heavily built environments where these features approach, or even cross, the edges of the channel as excessive post processing may be required. Similarly, it is not suitable for rivers, which traverse morphologically smooth landscapes including rivers in sand or ice.

Within these limitations, we hold that this technique represents a valuable tool for the quick and robust extraction of river bank locations from imagery of a large majority of the world's rivers when traditional land based surveys are either unavailable or unfeasible. The relative speed of image processing and the lack of reliance of any sort of specialized imagery make it suitable for times when project schedules or operational requirements do not allow for waiting to acquire more specialized imagery. Further, its fully automate nature make it suitable for unattended processing during times when human operators are unavailable.

ACKNOWLEDGEMENTS

This work was supported under the NRL 6.2 Core Project 'The Performance of a Persistent Riverine Surveillance Network'. The authors would like to thank Mr Bob Linzell for his assistance in testing the technique. We also thank the editor and the anonymous reviewers for their comments, which have greatly improved this paper. This is Naval Research Lab Contribution Number NRL-7320-13-1779.

REFERENCES

Alphan H. 2005. Perceptions of coastline change in river deltas: southeast Mediterranean coast of Turkey. *International Journal of Environment and Pollution* **1**(23): 99–102.

Awate S, Tasdizen T, Whitaker R. 2006. Unsupervised texture segmentation with nonparametric neighborhood statistics. *Proceedings of the European Conference on Computer Vision (ECCV).*

DOI: 10.1002/rra

Gilvear D, Davids C, Tyler A. 2004. The use of remotely sensed data to detect channel hydromorphology; River Tummel, Scotland. *River Research and Applications* **20**: 795–811.

Huang K. 2002. A synergistic automatic clustering technique (syneract) for multispectral image analysis. *Photogrammetric Engineering and Remote Sensing* **68**(1): 33–40.

Jensen J. 1996. *Introductory Digital Image Processing—A Remote Sensing Perspective*. Prentice Hall, Inc.: Upper Saddle River, NJ.

Kelley G, Hobgood J, Bedford K, Schwab D. 1998. Generation of three-dimensional lake model forecasts for Lake Erie. *Journal of Weather Forecasting* **13**: 305–315.

Legleiter C, Roberts D, Marcus A, Fonstad M. 2004. Passive optical remote sensing of river channel morphology and in-stream habitat: physical basis and feasability. *Remote Sensing of the Environment* **93**: 493–510.

Marcus A, Fonstad M. 2007. Optical remote mapping of rivers at sub-meter resolutions and watershed extents. *Earth Surface Processes and Landforms* **33**: 4–24.

Novikov A, Bagtzoglou A. 2006. Hydrodynamic model of the Lower Hudson River estuarine system and its application for water quality management. *Water Resources Management* **20**(2): 257–276.

Pasternak G, Wang C, Merz J. 2003. Application of a 2D hydrodynamic model to design of reach-scale spawning gravel replenishment on the Mokelume River, California. *River Research and Applications* **20**(2): 1–21.

Pharwaha A, Singh B. 2009. Shannon and non-Shannon measures of entropy for statistical texture extraction in digitized mammograms. *Proceedings of the World Congress on Engineering and Computer Science*. Vol. **2**.

Pratt W. 1991. *Digital Image Processing*. John Wiley and Sons: New York.

Sera J. 1983. *Image Analysis and Mathematical Morphology*. Academic Press: Maryland Heights, MO.

Shannon C. 1948. A mathematical theory of communication. *Bell Systems Technical Journal* **27**: 379–423.

Singh B, Singh A. 2008. Edge detection in gray level images based on Shannon entropy. *Journal of Computer Science* **4**: 186–191.

Tanaka H. 2006. Monitoring of short term morphology change at a river mouth. *Proceedings of the Vietnam-Japan Estuary Workshop*; 1–6.

Tuceryan M. 1994. Moment based texture segmentation. *Pattern Recognition Letters* **15**: 659–668.

Tuceryan M, Jain A. 1990. Texture segmentation using Vornoi polygons. *IEEE Transactions on Pattern Analysis and Machine Intelligence - PAMI12*; 211–216.

Tuceryan M, Jain A. 1998. Texture Analysis. In *Handbook of Pattern Recognition and Computer Vision*, Chen C, Paul L, Wang P (eds). World Scientific Publishing Co.: Singapore.

Vericat D, Brassington J, Wheaton J, Cowie M. 2009. Accuracy assessment of aerial photographs acquired using lighter-than-air blimps: low cost tools for mapping river corridors. *River Research and Applications* **25**(8): 985–1000.

Viyas V, Rege P. 2006. Automated texture analysis with Gabor filters. *Graphics, Visualization and Image Processing* **6**: 35–41.

Westaway R, Land S, Hicks D. 2003. Remote survey of large-scale braided, gravel bed rivers using digital photogrammetry and image analysis. *International Journal of Remote Sensing* **24**: 795–816.

Winterbottom S, Gilvear D. 1997. Quantification of channel bed morphology in gravel-bed rivers using airborne multispectral imagery and aerial photography. *Regulated Rivers: Research and Management* **13**: 489–499.

Yang L, Wang Y, Zhu Z. 2006. Three dimensional numerical model for winding tidal river with branches. *Journal of Hydrodynamics* **19**(2): 249–254.

DOI: 10.1002/rra